euronoise 2021
25th to 27th of October
Madeira, Portugal - online

Acoustic metamaterial for low frequency harmonic noise mitigation

Michal Kozupa[1], Beata Kotra[1]

[1]Hitachi ABB Power Grids, Krakow, Poland
michal.kozupa@hitachi-powergrids.com, beata.kotra@hitachi-powergrids.com

Abstract
Harmonic sound with strong low frequency component is often inherent in industrial noise such as ventilators, pumps, transformers, etc. Typical solutions for low frequency noise mitigation can be hampered by the required size or mass of the solution. However, when the noise have harmonic spectrum, resonance-based solutions are often used from which acoustic metamaterials are of great interest in the last years. In this paper design, FEM simulations and experimental validation of acoustic metamaterials for low frequency harmonic noise will be investigated. The design is based on zigzag shaped labyrinth structure for multiplication of the channels length. Such increased length and shape provide easier tuning for low frequencies and long wavelengths in limited volume. Later, numerical simulations of acoustic resonance and transmission loss are performed in Ansys Mechanical with shape optimization. Finally, optimized design is 3D printed and tested in impedance tube for insertion loss measurements.

Keywords: noise reduction, acoustic metamaterials, transmission loss, numerical simulations.

1 Introduction

Acoustic metamaterials (AMMs) are artificially engineered materials, structured to have unconventional effective properties that are usually not found in nature, which can be used to address engineering challenges in acoustics that don't have easily applicable conventional solutions, such as ultrathin acoustic absorbers, spatially compact acoustical lenses, acoustic cloaking, and many more [1]. One type of AMMs that have been widely studied in recent years are labyrinthine and space-coiling acoustic metamaterials. It has been experimentally proven that a properly designed labyrinthine acoustic metamaterial can exhibit attractive sound attenuating properties. What is more, they can shift the band of strong sound attenuation to desired frequencies by changing geometric features, therefore they are valuable for noise reduction applications [1].

In the 1990s, the concept of a phononic crystal was derived [3]. In 1992, Sigalas theoretically synthesized phononic crystals for the first time [5]. Kushwaha formally proposed that concept in 1993 [6]. The first and probably most widely known AMM, created by Liu in 2000 was designed to isolate low-frequency sound much more efficiently than the classical mass law [7]. In 2015, Li designed a curly space structure composed of a Jerusalem cross groove air matrix periodically arranged in a square lattice [8]. The same year, Wang designed an S-shaped structure in a square lattice. They found that the structure can produce a more complete and larger bandgap in the lower frequency than the structure proposed by Li, with the same lattice parameters [9]. In 2017, Xia designed a spatially coiled acoustic metamaterial based on the Hilbert fractal structure [10]. In 2019, Dong proposed a new structure with broadband double-negativity based on the cavity structure and spatial curling mechanism. The negative refraction and sub-wavelength imaging of the structure were numerically simulated [11].

In this paper, three types of space-coiling AMMs are designed, and their sound-blocking properties are tested through numerical simulations and later one shape is evaluated through measurement of a 3D printed sample. The results are presented and discussed.

2 Types of designed acoustic metamaterials

2.1 Zigzag Acoustic Metamaterial

First tested type of analyzed AMM is Zigzag Acoustic Metamaterial (ZZAMM) in which the sound wave propagates along the zigzag channels. Therefore the propagation length of the sound wave is greatly multiplied. Thanks to that phenomenon the effective sound speed in the Zigzag AMM is ultraslow compared to the background medium. The zigzag shape is created based on the Wunderlich curves which are a collection of plane-filling curves. The Wunderlich curve begins with an s-shape, and each successive iteration translates-rotates-reflects its copies in a 3×3 grid. In this paper, a few different size configurations of ZZAMM are tested based on previous works where the structures were found to have broadband sound blocking properties. The geometry can be described by 4 parameters: side length *a*, channel width *w*, internal wall length *L* and wall thickness *d* as presented on Figure 1. The next iterations are created by adding more internal walls creating zigzag channels of length $L/2^{N-1}$ where *N* is the iteration level. The proposed dimensions of ZZAMMs are presented in Table 1.

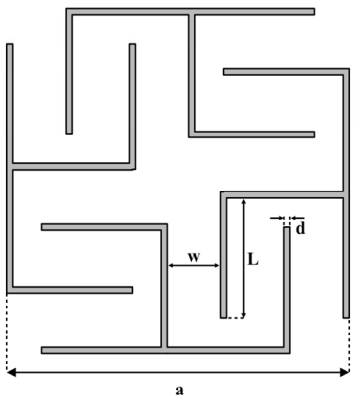

Figure 1 - Dimensions of ZZAMM unit cell.

Table 1 - Dimensions of proposed first-order to third-order ZZAMMs.

	First-order		**Second-order**		**Third-order**	
Lattice constant *a* [mm]	70	65	70	65	70	65
The thickness of solid walls *d* [mm]	1	1	1	1	1	1
Width of a passage between channels *w* [mm]	10,5	8	4	4	2	1.2
Internal wall length *L* [mm]	24.8	23	24.8	23	24.8	23

2.2 Hilbert Fractal Acoustic Metamaterial

Second tested type of Labyrinthine Acoustic Metamaterial is Hilbert Fractal Acoustic Metamaterial (HFAMM) whose geometry is based on the Hilbert Curve that generates an acoustic waveguide which significantly elongates the path that the sound wave propagates through [2]. The path of sound propagation is also iterated by increasing fractal order. As a result, coiling up space can be considered equivalent to an artificial medium with an ultraslow sound speed [13]. In this paper, a few different size configurations of HFAMM are designed and tested. HFAMM can be described by the dimensions presented on Figure 2. The proposed dimensions of HFAMMs are presented in Table 2.

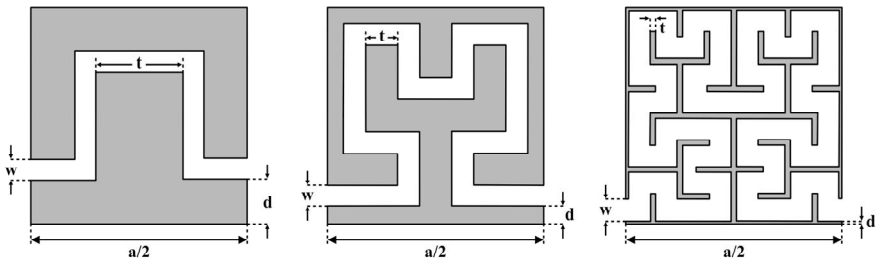

Figure 2 – HFAMM dimensions.

Table 2 - Dimensions of proposed first-order to third-order HFAMMs

	$a\,[mm]$	$w\,[mm]$	$t\,[mm]$	$d\,[mm]$
First order	70	4	31	15,5
	70	2	33	16,5
	65	4	28,5	14,25
	65	2	30,5	15,25
	60	2	26	13
Second order	70	4	13,5	6,75
	70	2	15,5	7,75
	65	4	12,25	6,125
	65	2	14,25	7,125
	60	4	11	5,5
	60	2	13	6,5
Third order	70	4	4,75	2,375
	70	2	6,75	3,375
	65	4	4,125	2,0625
	65	2	6,125	3,0625
	60	4	3,5	1,75

2.3 Spider Web inspired AMM

Third tested type of designed AMMs is Spider Web Inspired AMM (SWAMM). This structure type have been first proposed in 2015 [15] as ultra-sparse metasurface based on artificial Mie resonances and later developed [16]. The unit cell of SWAMM consists of a square external frame and a circular 'labyrinth' divided into either four or eight independent circular-shaped channels connected at the center. The schematic diagram of the SWAMM is presented on Figure 3 as well as the describing parameters of the geometry. Spider-web structured AMM geometries can be defined by seven parameters: the lattice constant *a*, the thickness of solid walls *d*, the length of side walls *l*, the radius of the internal cavity *r*, the width of a passage between channels *w* and the curling number *N* (or the number of circles used to create the curved channels).

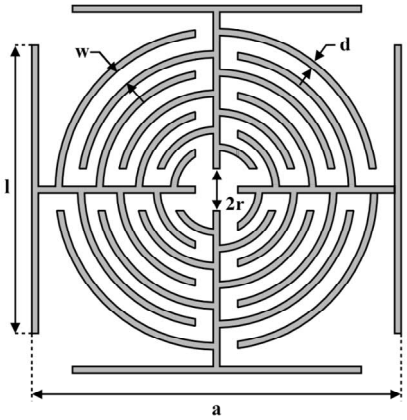

Figure 3 – SWAMM unit cell.

Based on previous works and limitations of size based on testing methods a few different size configurations of a unit cell are tested. The proposed dimensions are presented in Table 3.

Table 3 - Proposed dimensions of the unit cell.

Lattice constant a [mm]	70	70	65	65
The thickness of solid walls d [mm]	1	1	1	1
Length of side walls l [mm]	50	50	45	45
Radius of the internal cavity r [mm]	3	3	2.5	2.5
Width of a passage between channels h [mm]	3	3	2.5	2.5
Curling number N	7	7	7	7
Number of sections	4	8	4	8

3 Numerical simulations

The base concept of AMM is that only one unit cell needs to be designed in order to determine the sound manipulating properties of a larger sample. The fact that the effective parameters of a metamaterial can be determined using simple and efficient methods is one of the most powerful aspects of metamaterials [12].

3.1 Modal analysis and Mie resonances

It has been proven that in AMMs resonance modes such as monopole and multipole occur. The eigenstates of AMMs are studied by the Ansys Mechanical Acoustic Modal Analysis module. The monopole resonance can produce a negative bulk modulus, while the dipole resonance can generate a negative mass density. To obtain resonant frequencies as well as mode shapes of AMMs the air channels are modeled. The boundaries are set as Radiation Boundary to eliminate the influence of reflections. The pressure at the interconnection center of AMM with respect to air losses is investigated to confirm the monopole and dipole resonances occurring in structures (Mie resonances), associated with sound blocking behavior.

The Acoustic Harmonic Analysis module of Ansys Mechanical has been used to calculate the pressure magnification at the center of the unit cell. The acoustic pressure of amplitude 1 Pa is applied to obtain plane wave excitation. The sides of the channels are considered to be rigid to model sound-hard boundary between air and solid structure. The outside walls are set as Radiation Boundary to eliminate the influence of reflections. Thermo-Viscous Boundary is applied at channel walls as it has been proven that viscous-thermal losses should be considered [2].

3.2 Transmission characteristics

The Transmission Loss is obtained through simulation to test the sound attenuating properties of a single unit cell of AMM. Surface velocity of 0.5 m/s is applied normal to the left boundary of the unit cell. The sound transmission is only calculated in the x-direction at the left and right boundary (inlet and outlet) of the unit cell. Channel walls are set as rigid to simulate sound hard boundary between the solid structure of AMM and air. The air is lossy and viscous-thermal losses are taken into account. Outside walls are set as radiation boundaries. The transmission is tested in the range from 0 to 1000 Hz for all designed unit cells of all AMMs types.

3.3 Sound Pressure Field

The sound pressure field distributions of the metamaterial in a rectangular waveguide were investigated. First, the frequency response of SPL at the outlet of the waveguide is obtained. Then the SPL field distributions at a frequency corresponding to the lowest values are calculated. At last, the SPL is compared with the sound pressure distribution of a rigid square obstacle of the same size. The excitation of the pressure of 1 Pa is applied at the left boundary of the model. The channel walls and outside walls are set as rigid to simulate waveguide conditions. The air is lossy and thermo-viscous losses are considered.

4 Measurement procedure

Sample of HFAMM of first order has been produced by 3D print method and tested with the use of impedance tube for Transmission Loss values. The method used in this paper is in compliance with the E2611-17 standard method. It uses an impedance tube with a sound source connected to one end and the test sample mounted in the tube. For transmission loss, four microphones, at two locations on each side of the sample, are mounted. Plane waves are generated. The acoustic transfer matrix is calculated and the transmission loss is extracted [14]. The equipment used for the experiment is presented on Figure 4. The impedance tube was Brüel & Kjær Transmission Loss Tube Kit Type 4206-T with four ¼" Condenser Microphones Type 4187. The remaining elements of the setup were Generator, 4/2-ch. Input/Output Module Type 3109, Power Amplifier Type 2716C, and a Computer. The thickness of the sample was 65mm and the distances between microphones were equal to 50mm.

Figure 4 – Experimental equipment setup and metamaterial sample

5 Results

5.1 Modal Analysis and Mie Resonances

In all of the tested unit cells both monopole and dipole mode shapes occur. The first two resonant frequencies are shown in tables 4 - 6. The simulations of acoustic pressure magnification in the center of the unit cell have shown that the maximum occurs at the frequency close to the monopole resonance frequency. Therefore it can be assumed that these localized modes correspond to Mie resonances which within the designed metamaterial unit cells is due to the negative effective density and bulk modulus.

Table 4 - Frequencies of monopole and dipole modes of ZZAMMs.

The lattice constant [mm]	First-order		Second-order		Third-order	
	Monopole [Hz]	Dipole [Hz]	Monopole [Hz]	Dipole [Hz]	Monopole [Hz]	Dipole [Hz]
70	861.7	1827.1	599.7	1231.8	182.1	364.2
65	925.1	1851.8	625	1278.4	206.6	411.5

Table 5 - First two resonant frequencies of HFAMMs from first to third order.

Unit cell side length [mm]	Channel width [mm]	First-order		Second-order		Third-order	
		Monopole [Hz]	Dipole [Hz]	Monopole [Hz]	Dipole [Hz]	Monopole [Hz]	Dipole [Hz]
70	2	828.3	2651	622.2	1296.9	367.1	737.4
70	4	978.6	2591.8	583.8	1272.8	329.3	668.8
65	2	910.2	2848.8	675.5	1401.6	405.5	813.4
65	4	1070.3	2784.4	633	1372.6	357.4	725.2
60	2	1007.3	3078.9	690.6	1489.3	390.8	791.9

Table 6 - First two resonant frequencies of SWAMM from first to third order.

Unit cell side length [mm]	Number of sub-sections	Monopole [Hz]	Dipole [Hz]
70	4	446.4	932.3
70	8	817.6	1630.3
65	4	525.9	1096.5
65	8	977.6	1931

For all tested unit cells their resonant frequencies shift to lower bands with the increase of unit cell size length a and with decrease in channel width w.

Table 7 contains monopole and dipole mode shapes of designed AMMs.

Table 7 – Mode shapes of AMMs.

	ZZAMM	HFAMM	SWAMM
monopole	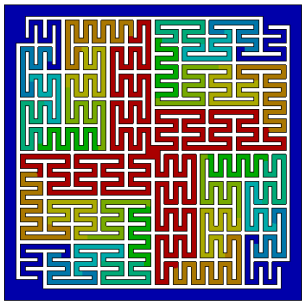	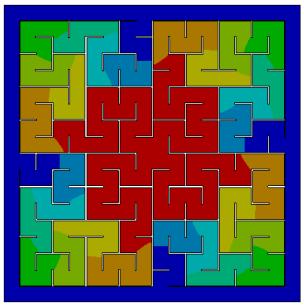	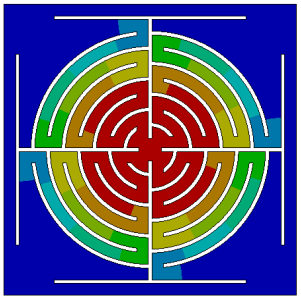
dipole	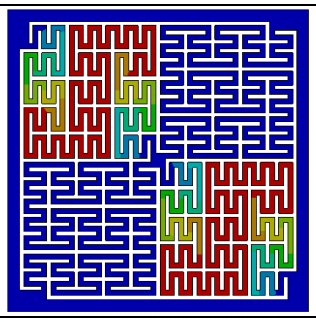	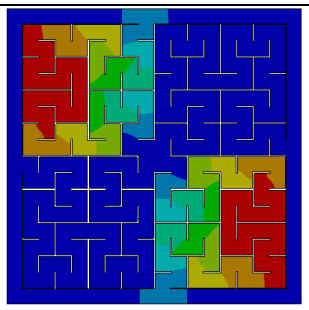	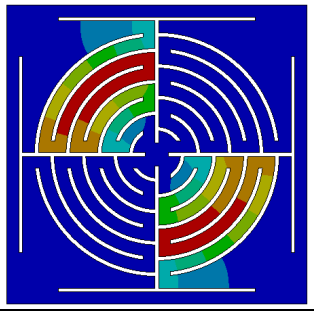

5.2 Transmission characteristics

Figure 5 presents comparison of Transmission Loss of three designed types of AMMs. This paper focuses on attenuation of harmonic noise with strong low frequency components. Therefore the TL values are presented for unit cells of side length a = 70mm and channel width w=2mm (third-order fractal of ZZAMM and HFAMM and SWAMM with 4 sub-sections) as for these dimensions the monopole and dipole frequencies were lowest for all metamaterial types. The chart shows that SWMM has lowest sound blocking properties and ZZAMM achieves highest values of TL. However the HFAMM has similarly high TL values with periodically occurring peaks and dips which is desirable for harmonic noise reduction. Based on these observation unit cell of HFAMM have been chosen for further testing.

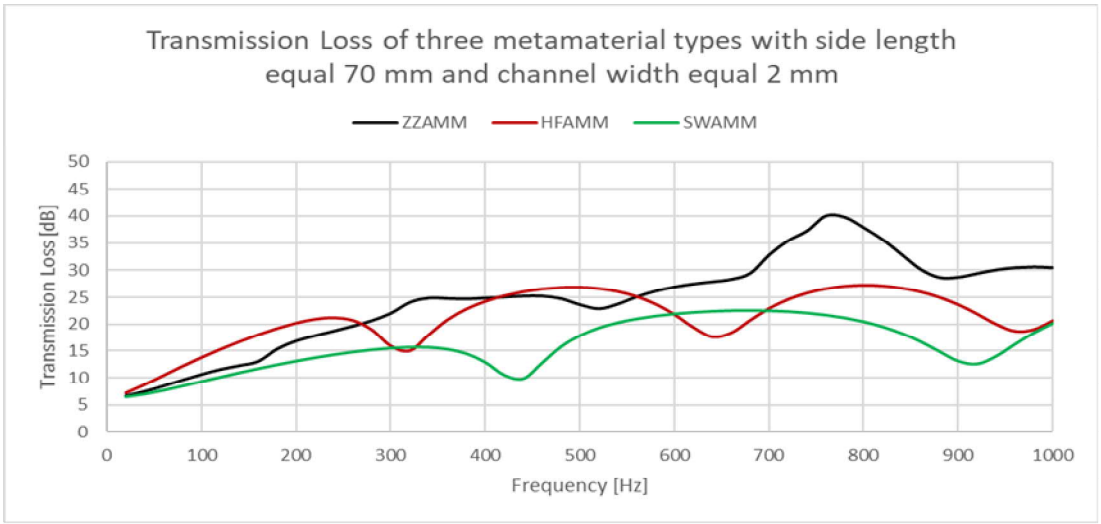

Figure 5 – Transmission Loss of three types of AMMs.

Sample of HFAMM of first order has been produced by 3D print method and tested with the use of impedance tube for Transmission Loss values. FEM simulation has been conducted with conditions that possibly best matched the measurement conditions. Both results are presented on Figure 6. In both cases, TL values are very low up to around 1500 Hz. Simulation data has a peak at 2280 Hz which perfectly aligns with experimental data, although for the second there is also a much larger peak at 2072 Hz. Above 2500 Hz TL rises with the frequency but simulation data is consequently lower. There are many reasons why the simulation and experimental data show such a significant difference. First, in simulation, the AMMs walls were set as rigid, while during the measurement the structures element were only fixed at one edge. What is more, the 3D printed model has the cylindrical element, which was not modeled in the simulation. However, the experimental results seem to be not only proving the capabilities of sound attenuating of the AMMs but also show that in real-life conditions it might have even better efficiency.

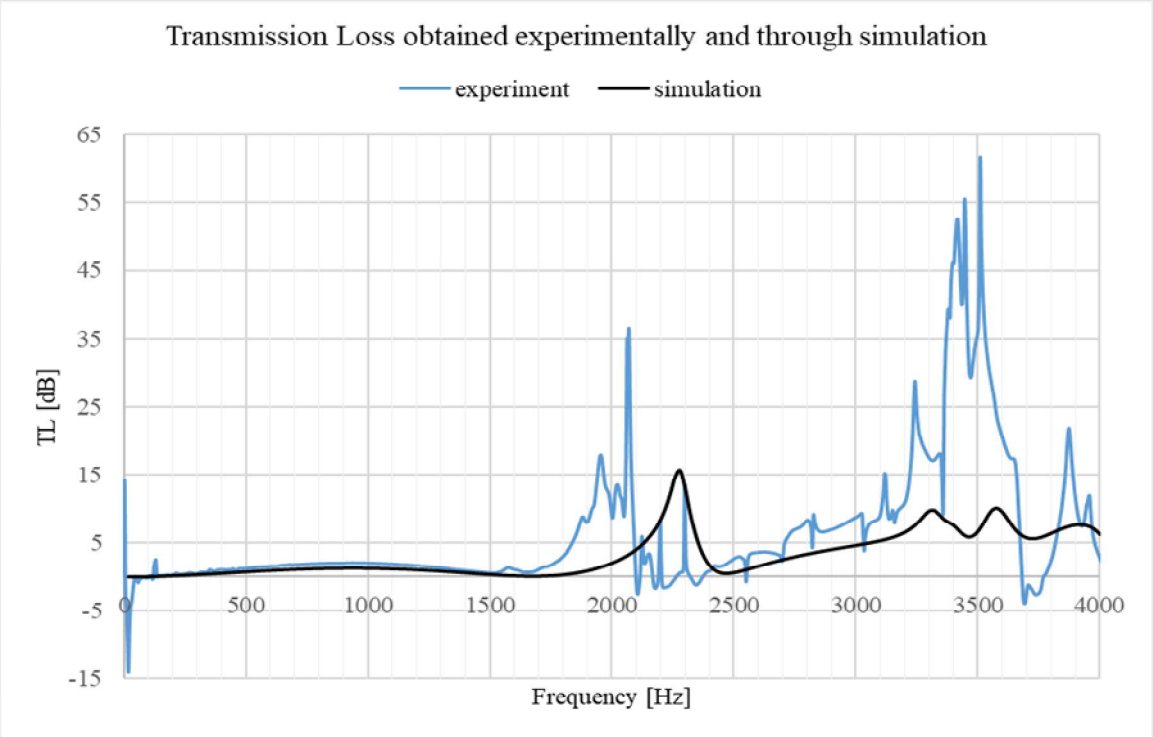

Figure 6 – TL values from measurement and simulation

5.3 Sound Pressure Field

Figure 7 presents Sound Pressure Level calculated at the outlet of a waveguide. First order unit cell has two peaks in the measured frequency range and in the narrow band the curve lays below that obtained for the solid block. With higher-order unit cells, more dips and peaks occur. The SPL lays below that measured for the solid block in a range of frequencies above 600 Hz for second-order and range from around 375 Hz to 700 Hz for third-order unit cells. Figure 8 shows SPL distributions in a waveguide with inserted unit cell of HFAMM of third order and solid obstacle at the frequency of 650 Hz. It can be observed that after the metamaterial the SPL has much lower values (around 60 dB) that in the case of a rigid obstacle (90 dB) which proves the sound-blocking capabilities of a metamaterial.

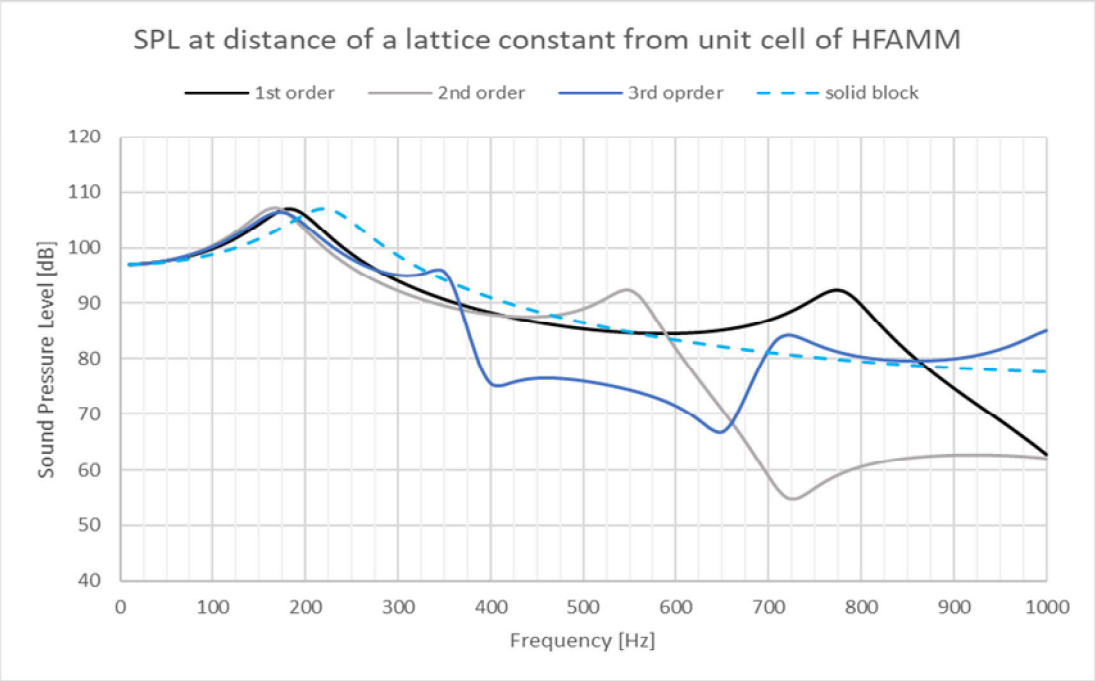

Figure 7 – SPL at a distance of a lattice constant from unit cell of HFAMM

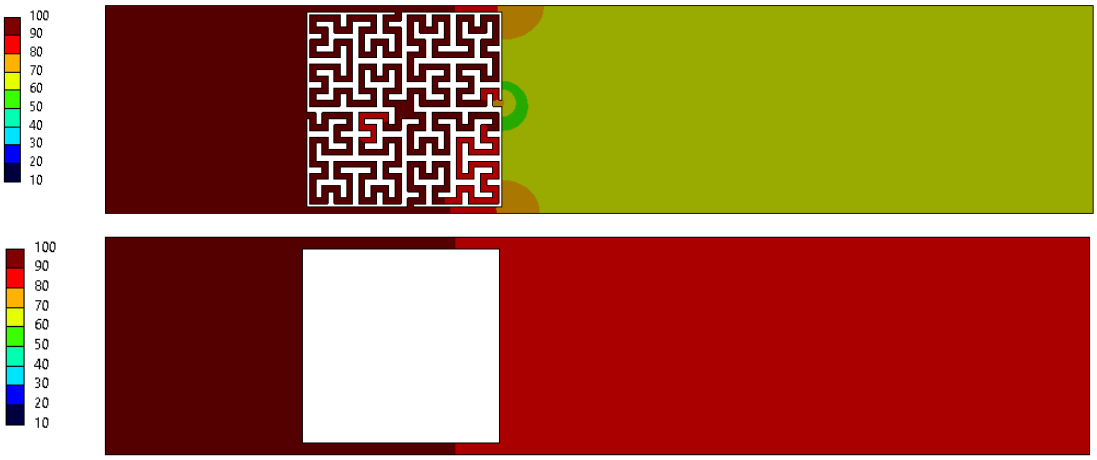

Figure 8 – SPL distributions in a waveguide

6 Conclusion

In this paper, three types of fractal inspired labyrinthine AMMs have been designed and their sound-attenuating properties have been investigated. The numerical results have demonstrated that the proposed AMMs can generate both the monopole and dipole modes and with the increase of the fractal order, the monopolar and bipolar resonances shift to the lower-frequency region. What is more, it has been found that the TL of the first-order to fourth-order HFAMMs and ZZAMMs increases with the decrease of the waveguide width w. The properties of a designed HFAMM of first-order have been tested with the use of a 3D printed sample for TL values. Comparing the numerical simulation results with measurement results, it is found that the values obtained through measurement are much higher but in the region of interest (below

1000 Hz), the TL is generally small. It can be caused by the absence of side walls closing the sample as in the simulations. It leads to a conclusion that these structures should be used and further tested with the side walls closing the channels. Furthermore, based on the method of selecting the optimal AMMs, we can easily design the AMMs suitable for the frequency bands of the noise that need to be reduced, therefore, there is a broad application prospect in the field of noise reduction, especially for low-frequency noise. Considering the problem of this work the HFAMM of third-order is most suitable for low-frequency harmonic noise reductions. Its TL values are highest from all tested AMMs and the sound insulation bands occur periodically. Generally bigger unit cell size and smaller waveguide width are recommended.

References

[1] M. R. Haberman, "Acoustic Metamaterials," *Acoustic Today*, pp. 31-39, 2016.

[2] X. Zhao, G. Liu, C. Zhang, D. Xia and Z. Lu, "Fractal acoustic metamaterials for transformer noise reduction," Beijing.

[3] J. Liu, H. Guo and T. Wang, "A review of Acoustic Metamaterials and Phononic Crystals," *Crystals*, vol. 10, 2020.

[5] M. Sigalas and E. N. Economou, "Elastic and acoustic wave band structure," Journal of Sound Vibration, vol. 158, pp. 377-382, 1992.

[6] M. S. Kushwaha, P. Halevi, L. Dobrzynski and B. D. Rouhani, "Acoustic band structure of periodic elastic composites," Physics review letters, vol. 71, pp. 2022-2025, 1993.

[7] X. Z. Y. M. Y. Y. Z. Z. Y. C. T. C. P. S. Zhengyou Liu, "Locally Resonant Sonic Materials," Science, 2000.

[8] Y. Li, T. Chen, X. Wang, K. Yu and R. Song, "Band structures in two-dimensional phononic crystals with periodic Jerusalem cross slot," Physica B: Condensed Matter, vol. 456, pp. 261-266, 2015.

[9] T. Wang, M.-p. Sheng, H. Wang and Q.-H. Qin, "Band structures in two-dimensional phononic crystals with periodic S-Shaped Slot," Acoustics Australia, vol. 43, pp. 275-281, 2015.

[10] B. Xia, T. LIU, S. ZHENG and Y. Dejie, "Coiling up space acoustic metamaterial with Hilbert fractal in a subwavelength scale," SCIENTIA SINICA Technologica, vol. 47, pp. 639-645, 2017.

[11] H.-W. Dong, S.-D. Zhao, P. Wei, Y.-S. Wang and C. Zhang, "Systematic design and realization of double-negative acoustic metamaterials by topology optimization," Acta Materialia, vol. 172, 2019.

[12] S. A. Cummer, J. Christensen and A. Alù, "Controlling sound with acoustic," NATURE REVIEWS, MATERIALS, 2016.

[13] X. Man, T. Liu, B. Xia, Z. Luo and L. Xie, "Space-coiling fractal metamaterial with multi-bandgaps on," Journal of Sound and Vibration, vol. 423, pp. 322-339, 2018.

[14] E2611−17: Standard Test Method for Normal Incidence Determination of Porous Material Acoustical Properties Based on the Transfer Matrix Method, 2017.

[40] C. Z. ,. B. G. Y. D. J. W. Q. W. X. J. L. Y. Cheng, "Ultra-sparse metasurface for high reflection of low-frequency sound based on artificial Mie resonances," Nature, Materials, 2015.

[41] A. Krushynska, F. Bosia, M. Miniaci and N. Pugno, "Spider web-structured labyrinthine acoustic metamaterials for low-frequency sound control," New Journal of Physics, vol. 19, 2017.